analytical chemistry

pubs.acs.org/ac Article

Versatile Electrochemiluminescence Biosensing Platform Based on DNA Nanostructures and Catalytic Hairpin Assembly Signal Amplification

Linying Yu, Liping Zhu, Yao Peng, Mengting Sheng, Jianshe Huang,* and Xiurong Yang*

Cite This: *Anal. Chem.* 2022, 94, 11368−11374 Read Online

ACCESS | Metrics & More | Article Recommendations | Supporting Information

ABSTRACT: Achieving rapid and highly sensitive detection of biomarkers is crucial for disease diagnosis and treatment. Here, a highly sensitive and versatile dual-amplification electrochemiluminescence (ECL) biosensing platform was constructed for target detection based on DNA nanostructures and catalyzed hairpin assembly (CHA). Specifically, when the target DNA was present, it would hybridize with the auxiliary strands (D1 and D2) to form an I-shaped nanostructure, which in turn triggered the subsequent catalytic hairpin assembly reaction to generate plenty of double-stranded DNA complexes (H1−H2). The resulting double-stranded complex could be trapped on the electrode surface and adsorbed the ECL signal probe $Ru(phen)_3^{2+}$.We found that the I-shaped nanostructure-triggered CHA reaction had higher amplification efficiency compared with traditional CHA amplification. Thus, a sensitive "signal-on" ECL biosensor was constructed for target DNA detection with a detection limit of 1.09 fM. Additionally, by combining the binding properties of C−Ag^+−C with an elaborately designed "Ag^+-helper" probe, the proposed strategy could be immediately utilized for the highly sensitive and selective detection of silver ions, demonstrating the versatility of the developed biosensing platform. This strategy provided a new approach with potential applications in disease diagnosis and environmental monitoring.

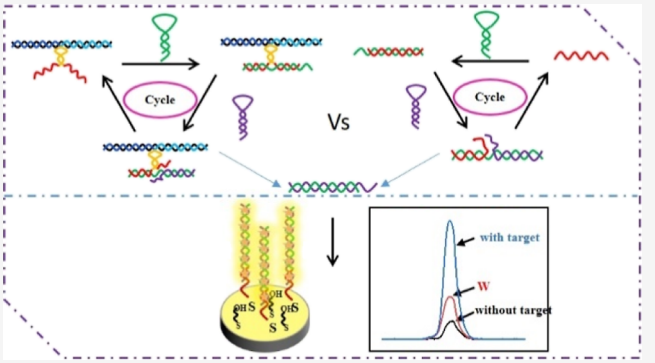

Achieving sensitive and specific detection of biomolecules is crucial for understanding the operating laws of life activities and realizing early diagnosis of diseases.[1,2] In recent years, various detection methods such as fluorescence, colorimetry, electrochemistry, and electrochemiluminescence (ECL) have been developed for biomarker detection.[3−6] Among them, ECL is widely used due to its high sensitivity, wide linear range, and temporal and spatial controllability.[7] However, due to the low abundance of biomarkers in real samples, it is still a major challenge to achieve highly sensitive detection for early diagnosis of diseases.

Varieties of isothermal DNA amplification techniques such as enzymatic cleavage-assisted cyclic amplification,[8] rolling circle amplification ,[9,10] hybrid chain reaction (HCR),[11] and catalytic hairpin self-assembly (CHA)[12] have been developed for constructing a sensing strategy due to the simplicity synthesis, low price, and high sequence predictability of nucleic acid. However, enzyme-assisted amplification requires the use of expensive equipment or encounters problems such as mutual interference between different enzyme cleavage reactions and enzyme inactivation in complex reactions during the experimental process, which limits its application.[13−15] In contrast, enzyme-free amplification strategies, especially CHA, have received extensive attention because the reaction can be performed under isothermal enzyme-free conditions.[16,17] For example, Fu et al. constructed an electrochemical sensor for the simultaneous detection of two RNAs by combining peptide nucleic acid and CHA.[18] However, although the CHA reaction can obtain large signal amplification, it still cannot meet the needs of the detection of some low-concentration biomarkers. To solve this problem, a strategy of combining CHA with other amplification methods was developed. For example, Wei et al. constructed a dual-amplification sensing strategy through the cascade of HCR and CHA achieving high-sensitivity detection of miRNA-141.[19] Chen et al. constructed a CHA multistage cascade strategy to achieve exponential signal amplification.[20] However, DNA leakage is unavoidable during the reaction, and the DNA cascade amplifies the leakage of the previous reaction, which will lead to an increased background signal. To solve this problem, the new CHA strategy with high speed and a high conversion rate was developed.[21,22] For

Received: May 25, 2022
Accepted: July 22, 2022
Published: August 4, 2022

https://doi.org/10.1021/acs.analchem.2c02239
Anal. Chem. 2022, 94, 11368−11374

example, Zhang et al. recently constructed a dual-catalyst hairpin assembly system through adding a DNA-excited strand to the traditional CHA reaction, making the reaction to have not only high reaction efficiency but also high reaction kinetics.[23]

DNA nanostructures are usually nanoscale structural materials with specific configurations formed by DNA self-assembly.[24,25] Since Fan's group reported that the sensing interface modified by DNA tetrahedral nanostructures (DTN) has higher capture efficiency than other DNA, DTN has been widely used in biosensing platforms.[26−30] Recently, Yuan's team designed a "crab claw" DNA nanomachine to achieve high-sensitivity detection of Hg^{2+}.[31] Since the cyclic amplification process is not involved in the formation process, the background signal can be reduced to a certain extent, which makes DNA nanostructures have great potential to participate in the construction of sensing strategies.

Inspired by the aforementioned results, we developed a novel DNA nanostructure-triggered CHA sensing strategy to achieve high-sensitivity detection of the targets (DNA or metal ions). Specifically, the presence of the target causes DNA hybridization with the auxiliary DNA to form the I-shaped DNA nanostructure, which subsequently triggers the CHA reaction to produce a great number of double-stranded DNAs (dsDNAs). Fluoresence and ECL experiments verified that the I-shaped DNA nanostructure-triggered CHA reaction had higher amplification efficiency than traditional CHA amplification. The produced dsDNAs were further anchored on the electrode surface through the capture probe to bind with ECL luminophore $Ru(phen)_3^{2+}$. Thus, a "signal-on" ECL biosensor was constructed to sensitively and specifically detect DNA or metal ions. The excellent analytical performance of the proposed biosensor demonstrated its promising applications in disease diagnosis and environmental monitoring.

EXPERIMENTAL SECTION

I-Shaped DNA-Triggered CHA Signal Amplification. All oligonucleotides (the sequences are shown in Table S1) were prepared as stock solutions (100 μM) with ultrapure water and diluted to a certain concentration with working buffer before use. THN buffer (0.01 M Tris−HCl solution, 0.1 M NaCl, pH 7.4) and TNN buffer (0.01 M Tris-HNO_3 solution, 0.1 M $NaNO_3$, pH 7.4) were used as working buffers for target DNA and Ag^+ detection, respectively. Prior to the reaction, hairpin DNA (H1 or H2) was annealed by heating at 95 °C for 5 min and cooling to 25 °C at a rate of 6 °C/min. Afterward, equal volumes of auxiliary strands (D1 and D2), different concentrations of the target, H1, and H2 were mixed at a final concentration of 1 μM and reacted at 37 °C for 2 h.

Fabrication of the ECL Biosensor. The glassy carbon electrode (GCE) was cleaned and AuNPs were electrodeposited according to our previously reported method.[32] Then, 10 μL of the 10 μM capture probe (H3) was incubated with 1 mM TCEP at 37 °C for 40 min to break disulfide bonds. Subsequently, 10 μL of pretreated H3 (1 μM) was carefully dropped on the electrode surface and incubated overnight at 4 °C. After washing three times with ultrapure water, the electrode was further incubated with 6 μL of MCH (1 mM) for 50 min at room temperature. After rinsing with ultrapure water, the CHA products were added on the surface of the electrode and reacted at 37 °C for 90 min. Next, the modified electrode was washed three times with ultrapure water and incubated with 500 μM $Ru(phen)_3^{2+}$ at 37 °C for 2 h. Ultimately, the obtained ECL biosensor was washed three times with ultrapure water and stored at 4 °C for subsequent experiments.

ECL Measurement Procedure. The constructed ECL biosensor was detected in 5.0 mL of the PBS solution (0.10 M PBS, 0.1 M KCl, pH 7.4) containing 20 mM 2-(dibutylamino) ethanol (DBAE). ECL test was performed in the potential range from 0 to 1.4 V with a scan rate of 0.1 V/s and a photomultiplier tube (PMT) voltage of 750 V.

Fluorescence Measurements. In order to evaluate the amplification effect of the I-shaped DNA nanostructure, a hairpin DNA LH2 was designed by labeling H2 with a fluorophore (FAM) at the 5′-end and a quencher (DABCYL) at the 3′-end. In the presence of the target, the double-stranded complex (H1-LH2) was formed after the CHA reaction, leading to the separation of the FAM/Dabcyl pair and the recovery of the fluorescent signal. Specifically, different concentrations of the target were mixed with D1, D2, H1, and LH2 and then reacted at 37 °C for 2 h. In the control experiment, single-strand DNA (W) was directly used to trigger CHA reaction between H1 and LH2 under the same conditions. When the CHA reaction was completed, the solution was diluted to 200 μL with a final concentration of 0.25 μM for fluorescence test. The fluorescence emission spectrum was acquired in the wavelength range from 490 to 600 nm with an excitation wavelength of 480 nm, and both the excitation and emission slit widths were set to 5 nm.

RESULTS AND DISCUSSION

Principle of the Proposed Biosensing Strategy. We propose a dual-amplification ECL sensing strategy based on the DNA nanostructure and CHA, which was programmable for multiple species detection with high sensitivity. As shown in Scheme 1, when the target DNA was present, it would hybridize with the auxiliary DNA (D1 and D2) to form an I-shaped DNA nanostructure that made the noncomplementary parts of D1 and D2 close to each other and acted as a primer to trigger the CHA reaction to generate the double-stranded complex (H1−H2). The resulting double-stranded complexes could be captured by the capture probe on the electrode surface. Subsequently, according to the property that $Ru(phen)_3^{2+}$ could be intercalated into the groove of double-stranded DNA, a "signal-on" ECL biosensor was constructed.

Scheme 1. Schematic Illustration of the Double-Amplified ECL Biosensor for Target DNA Detection. (A) Reaction Process of the Catalytic Hairpin Self-Assembly and (B) Assembly Process on the Electrode Surface

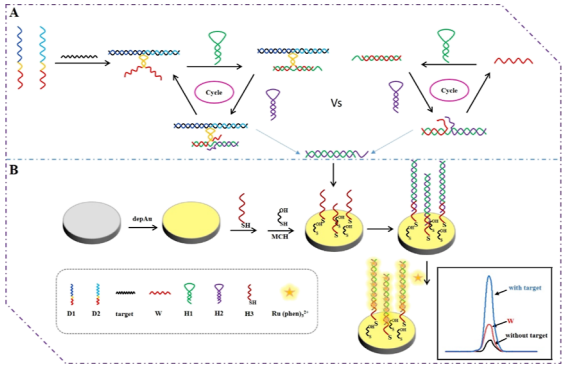

https://doi.org/10.1021/acs.analchem.2c02239
Anal. Chem. 2022, 94, 11368−11374

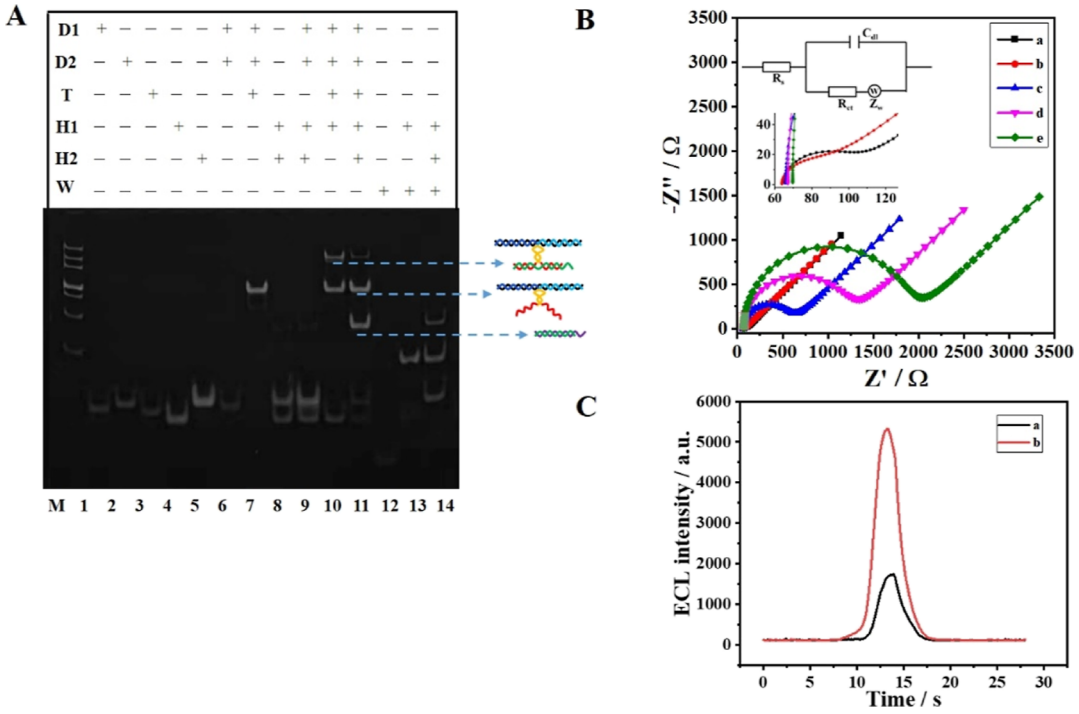

Figure 1. (A) PAGE characterization of the I-shaped DNA nanostructure assembly and CHA cycle amplification process. (B) EIS curves of layer-by-layer modification of the electrode surface: (a) GCE, (b) depAu/GCE, (c) H3/depAu/GCE, (d) MCH/H3/depAu/GCE, and (e) H1−H2/MCH/H3/depAu/GCE. The concentration of target DNA was 1 nM. (C) ECL response curves to target DNA: (a) 0 and (b) 1 pM.

In addition, to demonstrate the amplification effect of I-shaped DNA nanostructures, we used the single-stranded probe W (the same DNA sequence as D1 and D2 to trigger H1) to directly trigger H1 and H2 for CHA cycle amplification. The results demonstrated that the I-shaped DNA nanostructure-triggered CHA reaction had higher reaction efficiency than single-stranded DNA-triggered CHA, vide infra. Based on the synergistic effect of DNA nanostructures and CHA, a cascaded sensing platform for highly sensitive detection of targets was constructed.

Feasibility Analysis. To prove the feasibility of the sensing strategy, the assembly of the I-shaped DNA nanostructure and the CHA amplification process were first characterized by native polyacrylamide gel electrophoresis (PAGE) (Figure 1A). Bands in lanes 1−5 correspond to D1, D2, target DNA (T), H1, and H2, respectively. In the absence of the target, D1 and D2 did not react and could coexist stably (lane 6). After adding the target, the corresponding single-stranded DNA band disappeared along with the appearance of a new band with slow migration velocity (lane 7), indicating that the single-stranded DNA was successfully assembled to form the DNA nanostructure. Line 10 represents I-shaped DNA nanostructures complexing with hairpin H1. The formed DNA nanostructures could catalyze the CHA reaction between H1 and H2 to form plenty of H1−H2 complexes (lane 11). In contrast, only a small amount of H1−H2 complex was generated for the mixture of W, H1, and H2 (lane 14), indicating that I-shaped DNA nanostructures had higher amplification efficiency. Additionally, a slight leakage was observed in lanes 8 and 9, which was negligible compared to the target-triggered reaction product, indicating that the formed I-shaped DNA nanostructures could efficiently trigger the CHA cycle amplification reaction. Comparing lane 10 and lane 13, it seems that the I-shaped DNA nanostructure had a lower reaction efficiency with the H1 probe due to the steric hindrance effect of the large size of DNA nanostructures. However, the nanostructure-mediated CHA reaction showed higher conversion efficiency than that of single-stranded DNA-triggered CHA (lane 11 vs lane 14). It is speculated that although the DNA nanostructure reduced the binding efficiency with H1, it also made the base pairing in a relatively relaxed state, thereby reducing the Gibbs free energy of the subsequent reaction with H2 and subsequently improving the conversion efficiency of the CHA reaction. These results demonstrate the feasibility of the I-shaped DNA nanostructure-triggered CHA amplification strategy.

Electrochemical impedance spectroscopy (EIS) was measured to characterize the layer-by-layer assembly process on the electrode surface during sensor construction. As shown in Figure 1B, the cleaned glassy carbon electrode had small arc-like impedance (curve a). After the surface of the glassy carbon electrode was modified with gold nanoparticles (depAu/GCE), the impedance was further decreased because the gold nanoparticles increased the conductivity of the electrode (curve b). When capture probe H3 was modified on the electrode surface, the impedance increased to 650 Ω (curve c), which was ascribed to the fact that the electrostatic repulsion between the negatively charged DNA and $[Fe(CN)_6]^{3-/4-}$ hindered the electron transfer. After blocking the electrode with MCH, the impedance increased to 1350 Ω (curve d). This was attributed to the fact that the formed MCH capping layer hindered the diffusion of $[Fe(CN)_6]^{3-/4-}$ to the electrode surface. After the electrode was incubated with the target-induced CHA reaction products, the impedance was further increased to 2000 Ω (curve e). This was consistent with the expected results, indicating that the generated double-stranded DNA (H1−H2) was successfully assembled to the electrode surface. The ECL signal in the presence and absence of the

https://doi.org/10.1021/acs.analchem.2c02239
Anal. Chem. 2022, 94, 11368−11374

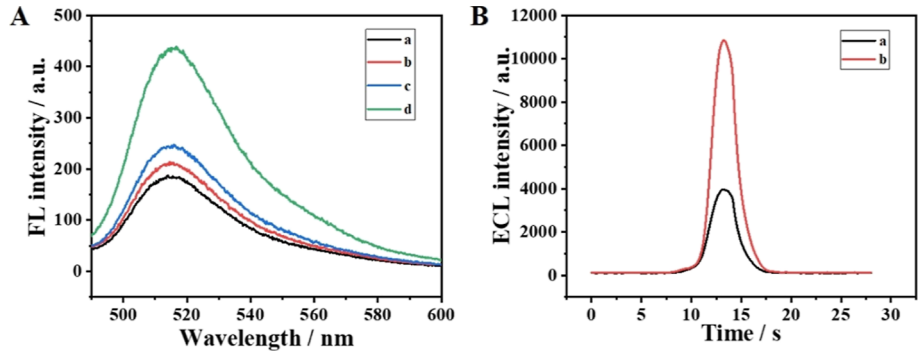

Figure 2. (A) Fluorescence spectra of (a) H1+LH2, (b) D1+D2+H1+LH2, (c) W + H1+LH2, and (d) target DNA + D1+D2+H1+LH2. (B) ECL response curve of single-stranded DNA (a) and I-shaped DNA nanostructure (b)-triggered CHA product-modified electrode, and the concentration of target DNA was 10 nM.

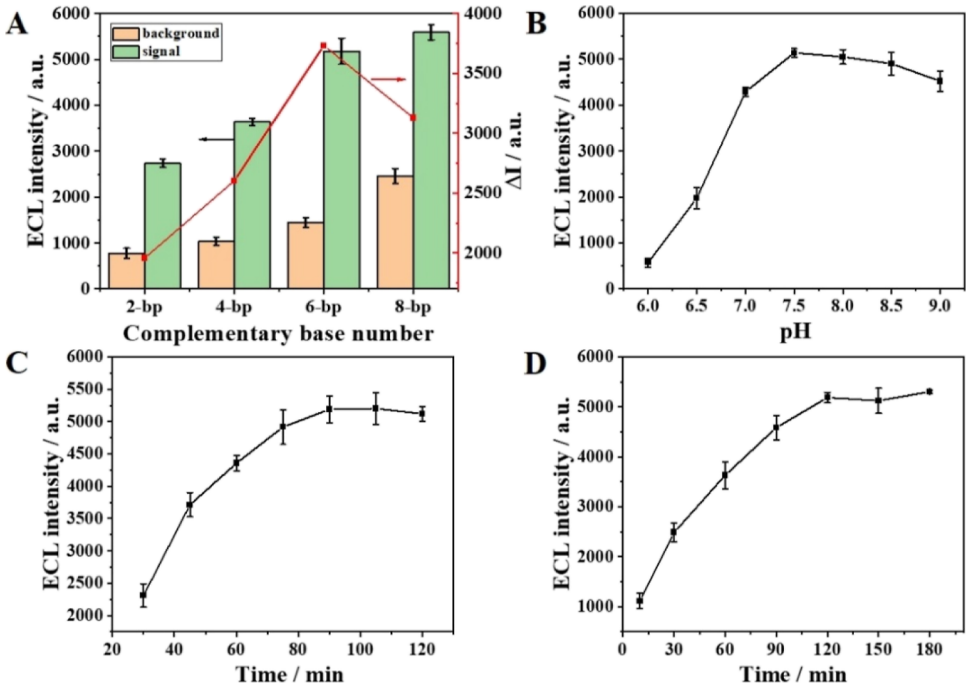

Figure 3. Optimization of the (A) number of complementary bases between D1 and D2, (B) pH of DBAE solution, (C) incubation time of H1−H2 with H3, and (D) time of dsDNA adsorption of $Ru(phen)_3^{2+}$. The concentration of target DNA was 1 pM.

target was compared to further demonstrate the feasibility of the experiment (Figure 1C). Only a low background signal was observed in the absence of target DNA (curve a). However, the sensor produced a significant signal response when 1 pM target DNA was present (curve b). These results all demonstrate the feasibility of the constructed sensing strategy.

Amplification Efficiency Characterization of I-Shaped DNA Nanostructures. Fluorescence and ECL were measured to demonstrate the amplification efficiency of I-shaped DNA nanostructure-triggered CHA reaction compared with the single-stranded DNA counterpart. As shown in Figure 2A, the fluorescence signal increased slightly after only the auxiliary probes D1 and D2 were added into the mixture solution of H1 and LH2 (curve b), indicating the ignorable leakage of the designed DNA probes. When single-stranded probe W was used to trigger the CHA reaction, only a little increase in fluorescence signal was observed (curve c). In stark contrast, when the target DNA was added to form I-shaped DNA nanostructures with D1 and D2, the resulting fluorescence signal was significantly increased, demonstrating the high amplification efficiency (curve d). From Figure 2B, we can see that the ECL experimental results are consistent with fluorescence experiment, and the ECL response signal generated by I-shaped DNA nanostructure-triggered CHA products (curve b) was approximately 2.8 times that of the single-stranded W probe (curve a). These results successfully demonstrated the high amplification efficiency of the I-shaped DNA nanostructure-triggered CHA.

Optimization of Experimental Conditions. The number of complementary base between D1 and D2 will significantly affect the subsequent reaction. If the complementary sequence is too short, steric hindrance will affect the proximity of H1 to the recognition sequences of D1 and D2, resulting in the decrease in the CHA reaction efficiency. However, if the complementary sequences of D1 and D2 are too long, the subsequent CHA reaction will spontaneously occur even without the participation of the target, resulting in an obvious background signal. Therefore, we first optimized the number of complementary bases between D1 and D2. As shown in Figure 3A, the ΔI (ΔI was the difference in the ECL

https://doi.org/10.1021/acs.analchem.2c02239
Anal. Chem. 2022, 94, 11368−11374

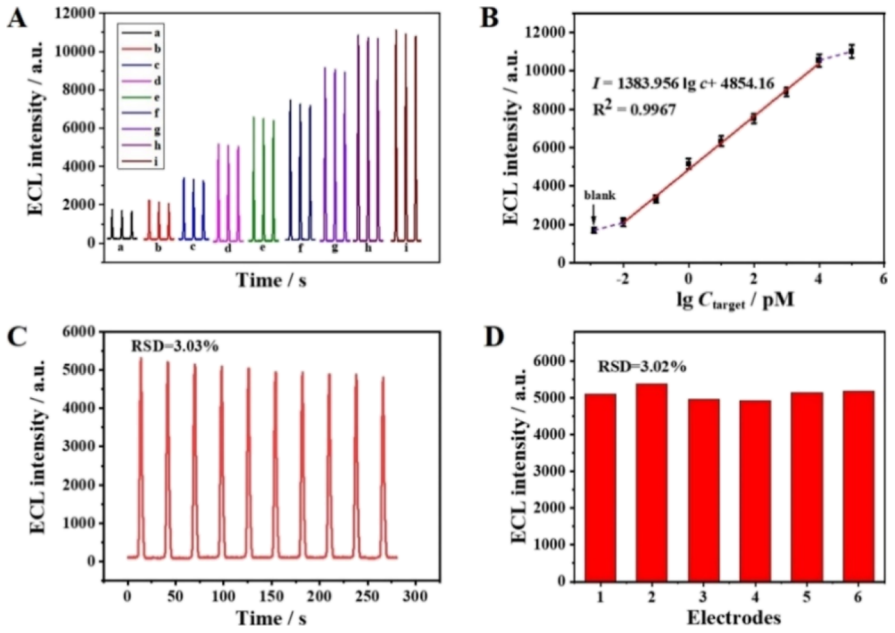

Figure 4. (A) ECL response curves to target DNA (From a−i: 0, 10, and 100 fM, 1, 10, and 100 pM, and 1, 10, and 100 nM). (B) Plot of the ECL intensity versus the logarithm of DNA concentration. (C) ECL response curve of successive 10 cycles and (D) ECL intensity of six parallelly fabricated biosensors. The concentration of target DNA was 1 pM.

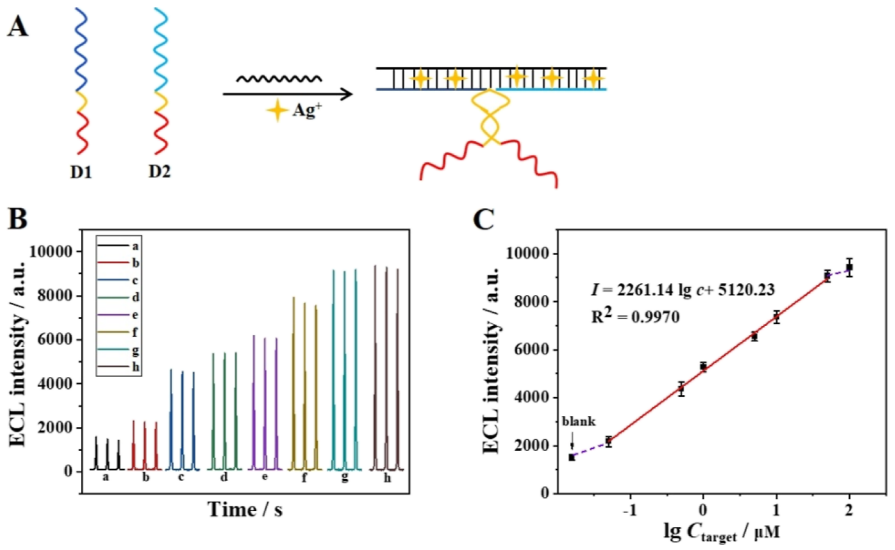

Figure 5. (A) Assembly process of I-shaped DNA nanostructures for Ag^+ detection. (B)ECL response curves to Ag^+ (From a−h: 0, 50, and 500 nM and 1, 5, 10, 50, and 100 μM). (C) Calibration plot of ECL intensity vs lg C_{Ag+}.

intensity between the signal and background) first increases with the increase in the complementary base number, and the maximum is obtained when six complementary bases (D1-3) exist between D1 and D2. Therefore, we chose the D1-3 sequence (Table S1) for subsequent experiments. After that, the pH of DBAE solution, incubation time of the H1−H2 complex with H3 on the electrode, and the time of dsDNA adsorption of $Ru(phen)_3^{2+}$ were optimized. The optimal experimental conditions of pH 7.4 (Figure 3B), 90 min incubation time (Figure 3C), and 2 h adsorption time (Figure 3D) were selected for subsequent experiments.

Analytical Performance for Target DNA. Under the optimal assay conditions, the target DNA was quantitatively analyzed using this biosensor. ECL intensity gradually enhanced with the increase in target DNA concentration (Figure 4A). The logarithm of DNA concentration in the range of 10 fM−10 nM had a good linear correlation (R^2 = 0.9967) with ECL intensity, and the detection limit was 1.09 fM (Figure 4B). Due to the high amplification efficiency of the CHA reaction triggered by the I-shaped DNA nanostructure, the proposed biosensor showed better or equivalent analytical performance in comparison with the previously reported DNA/RNA biosensors (Table S2).

The stability of the biosensor was evaluated by successively scanning for 10 cycles. As shown in Figure 4C, the ECL intensity does not change significantly with a relative standard deviation (RSD) of 3.03% (n = 10). It showed that the sensor has good stability. Reproducibility is another important index to evaluate the performance of the biosensor. When the target DNA concentration was 1 pM, the measured RSD of six

https://doi.org/10.1021/acs.analchem.2c02239
Anal. Chem. 2022, 94, 11368−11374

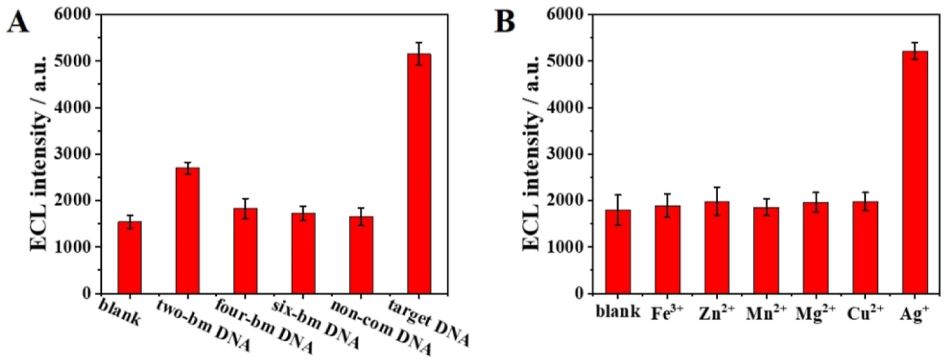

Figure 6. Specificity of the ECL sensor for (A) target DNA and (B) Ag^+. The concentration of target DNA and base-mismatched DNAs was 1 pM, and the concentration of Ag^+ and interfering ions was 1 μM.

electrodes was 3.02% (Figure 4D), indicating good fabrication reproducibility. Recovery experiments were performed in 10% human serum samples to evaluate the sensor's application potential. As shown in Table S3, the recoveries are calculated to be 92.02−101.62% with an RSD of 2.07−3.26%, proving the potential application of the biosensor in clinical sample detection.

Detection of Ag^+. The proposed biosensing strategy can be used not only for target DNA detection but also for detecting other targets such as proteins and metal ions. We take Ag^+ detection as an example to demonstrate the flexibility of this sensing strategy. The specific design process is shown in Figure 5A. In the presence of Ag^+, the C-rich sequence (Ag^+-helper) forms an I-shaped DNA nanostructure with D1 and D2 through C−Ag^+−C coordination interaction. The formed I-shaped DNA nanostructure was further used to trigger CHA reaction; thus, an ECL biosensor was developed for Ag^+ detection (Scheme 1). As shown in Figure 5B, the ECL intensity was enhanced as the Ag^+ concentration increased. There is a good linear correlation between ECl intensity and the logarithm of Ag^+ concentration in the range of 50 nM−50 μM (R^2 = 0.9970), and the detection limit was calculated to be 0.68 nM (Figure 5C). Compared with other Ag^+ sensors, this biosensor exhibited a wider linear range and comparable detection limit (Table S2). This result also demonstrated the versatility of the proposed biosensing strategy for different target detection.

Specificity Study. The selectivity of the biosensor to target DNA or Ag^+ was evaluated. DNA sequences with 2, 4, and 6 mismatched bases and noncomplementary DNA were selected to investigate the selectivity of the sensor to target DNA (Figure 6A), and metal ions (Fe^{3+}, Zn^{2+}, Mn^{2+}, Mg^{2+}, and Cu^{2+}) were selected to investigate the selectivity of the sensor to Ag^+ (Figure 6B). Only in the presence of target DNA or Ag^+, the ECL intensity was enhanced, indicating that the sensor has good selectivity for target DNA and Ag^+.

CONCLUSIONS

In summary, we combined DNA nanostructures and catalytic hairpin self-assembly to develop a highly sensitive electrochemiluminescence sensing system for DNA and Ag^+ detection. This sensing strategy has the following advantages: (1) The CHA reaction is an isothermal and enzyme-free amplification strategy, and the amplification process is carried out in solution, which simplifies the operation steps and improves the detection efficiency. (2) The I-shaped nanostructure-triggered CHA reaction had higher amplification efficiency compared with traditional CHA amplification, thus improving the detection sensitivity. (3) The sensing strategy is programmable and can be used for other target detection by simply changing the recognition sequence of the I-shaped DNA nanostructures. Based on the abovementioned advantages, this sensing strategy shows excellent sensitivity and specificity for both target DNA and Ag^+ detection, which provides a new avenue for disease and environmental detection.

ASSOCIATED CONTENT

Supporting Information

The Supporting Information is available free of charge at https://pubs.acs.org/doi/10.1021/acs.analchem.2c02239.

Reagents, apparatus, PAGE analysis, sequences of oligonucleotides used in this study, comparison of the analytical results of the proposed biosensor for target detection with previously reported strategies, and recovery for target DNA detection in real human serum (PDF)

AUTHOR INFORMATION

Corresponding Authors

Jianshe Huang − *State Key Laboratory of Electroanalytical Chemistry, Changchun Institute of Applied Chemistry, Chinese Academy of Sciences, Changchun 130022, China*; Phone: +86 431 85262964; Email: huangjs@ciac.ac.cn; Fax: +86 431 85689278

Xiurong Yang − *State Key Laboratory of Electroanalytical Chemistry, Changchun Institute of Applied Chemistry, Chinese Academy of Sciences, Changchun 130022, China; University of Science and Technology of China, Hefei 230026, China*; orcid.org/0000-0003-0021-5135; Phone: +86 431 85262964; Email: xryang@ciac.ac.cn; Fax: +86 431 85689278

Authors

Linying Yu − *State Key Laboratory of Electroanalytical Chemistry, Changchun Institute of Applied Chemistry, Chinese Academy of Sciences, Changchun 130022, China; University of Science and Technology of China, Hefei 230026, China*

Liping Zhu − *University of Science and Technology of China, Hefei 230026, China*

Yao Peng − *University of Science and Technology of China, Hefei 230026, China*

Mengting Sheng − *University of Science and Technology of China, Hefei 230026, China*

Complete contact information is available at: https://pubs.acs.org/10.1021/acs.analchem.2c02239

Author Contributions

The manuscript was written through contributions of all authors.

Notes

The authors declare no competing financial interest.

■ ACKNOWLEDGMENTS

This work was supported by the National Natural Science Foundation of China (nos. 22034006, and 21721003), the Key Research Program of Frontier Sciences, and CAS (QYZDY-SSW-SLH019).

■ REFERENCES

(1) Zhou, H.; Liu, J.; Xu, J. J.; Zhang, S. S.; Chen, H. Y. *Chem. Soc. Rev.* **2018**, *47*, 1996−2019.
(2) Sun, Y.; Fang, L.; Zhang, Z.; Yi, Y.; Liu, S.; Chen, Q.; Zhang, J.; Zhang, C.; He, L.; Zhang, K. *Anal. Chem.* **2021**, *93*, 7516−7522.
(3) Lu, S.; Hu, T.; Wang, S.; Sun, J.; Yang, X. *ACS Appl. Mater. Interfaces* **2017**, *9*, 167−175.
(4) Chen, W. W.; Zhang, X. B.; Li, J. J.; Chen, L. Z.; Wang, N. N.; Yu, S. Q.; Li, G. M.; Xiong, L. F.; Ju, H. X. *Anal. Chem.* **2020**, *92*, 2714−2721.
(5) Ling, P. H.; Lei, J. P.; Zhang, L.; Ju, H. X. *Anal. Chem.* **2015**, *87*, 3957−3963.
(6) Li, J.; Luo, M.; Jin, C.; Zhang, P.; Yang, H.; Cai, R.; Tan, W. *ACS Appl. Mater. Interfaces* **2022**, *14*, 383−389.
(7) Liu, Z. Y.; Qi, W. J.; Xu, G. B. *Chem. Soc. Rev.* **2015**, *44*, 3117−3142.
(8) Wang, Q.; Liu, Y.; Wang, X.; Wang, F.; Zhang, L.; Ge, S.; Yu, J. *ACS Appl. Mater. Interfaces* **2021**, *13*, 25783−25791.
(9) Lin, Y.; Huang, X.; Zhang, Y.; Chen, D.; Wang, J.; Luo, F.; Guo, L.; Qiu, B.; Lin, Z. *Chemelectrochem* **2019**, *6*, 827−833.
(10) Zhang, H.; Zhuo, Z.; Chen, L.; Chen, C.; Luo, F.; Chen, Y.; Guo, L.; Qiu, B.; Lin, Z.; Chen, G. *Electrochem. Commun.* **2018**, *88*, 75−78.
(11) Zhu, L.; Ye, J.; Yan, M.; Zhu, Q.; Wang, S.; Huang, J.; Yang, X. *ACS Sens* **2019**, *4*, 2778−2785.
(12) Zhu, L.; Zhang, M.; Ye, J.; Yan, M.; Zhu, Q.; Huang, J.; Yang, X. *Anal. Chem.* **2020**, *92*, 8614−8622.
(13) Xia, L. Y.; Li, M. J.; Wang, H. J.; Yuan, R.; Chai, Y. Q. *Anal. Chem.* **2020**, *92*, 14550−14557.
(14) Lv, H.; Chen, A.; Cheng, W.; Kong, L.; Zhao, M.; Ding, S.; Ju, H.; Cheng, W. *Anal. Chem.* **2020**, *92*, 15624−15631.
(15) Yu, S.; Wang, Y.; Jiang, L. P.; Bi, S.; Zhu, J. J. *Anal. Chem.* **2018**, *90*, 4544−4551.
(16) Cui, L.; Zhou, J.; Yang, X. Y.; Dong, J.; Wang, X.; Zhang, C. Y. *Chem. Commun.* **2020**, *56*, 10191−10194.
(17) Zhang, Y.; Yan, Y.; Chen, W.; Cheng, W.; Li, S.; Ding, X.; Li, D.; Wang, H.; Ju, H.; Ding, S. *Biosens. Bioelectron.* **2015**, *68*, 343−349.
(18) Fu, P.; Xing, S.; Xu, M J.; Zhao, Y.; Zhao, C. *Sens. Actuators, B* **2020**, *305*, 127545.
(19) Wei, Y.; Zhou, W.; Li, X.; Chai, Y.; Yuan, R.; Xiang, Y. *Biosens. Bioelectron.* **2016**, *77*, 416−420.
(20) Chen, X.; Briggs, N.; McLain, J. R.; Ellington, A. D. *Proc. Natl. Acad. Sci. U. S. A.* **2013**, *110*, 5386−5391.
(21) He, Z. Q.; Wu, J.; Qiao, B.; Pei, H.; Xia, Q. F.; Wu, Q.; Ju, H. X. *ACS Appl. Bio Mater.* **2020**, *3*, 5342−5349.
(22) Liu, W. W.; Zhang, X. L.; Zhu, L.; Xu, S.; Chai, Y. Q.; Li, Z. H.; Yuan, R. *Anal. Chim. Acta* **2022**, *1204*, 339663.
(23) Zhang, X. L.; Yin, Y.; Du, S. M.; Kong, L. Q.; Yang, Z. H.; Chang, Y. Y.; Chai, Y. Q.; Yuan, R. *Adv Sci* **2022**, *9*, 2104084.
(24) Li, F.; Li, J.; Dong, B.; Wang, F.; Fan, C.; Zuo, X. *Chem. Soc. Rev.* **2021**, *50*, 5650−5667.
(25) Yin, J.; Xie, M.; Wang, J.; Cui, M.; Zhu, D.; Su, S.; Fan, C.; Chao, J.; Li, Q.; Wang, L. *Small* **2022**, *18*, No. e2200824.
(26) Lu, N.; Pei, H.; Ge, Z. L.; Simmons, C. R.; Yan, H.; Fan, C. H. *J. Am. Chem. Soc.* **2012**, *134*, 13148−13151.
(27) Ge, Z. L.; Gu, H. Z.; Li, Q.; Fan, C. H. *J. Am. Chem. Soc.* **2018**, *140*, 17808−17819.
(28) Zhu, L. P.; Ye, J.; Wang, S.; Yan, M. X.; Zhu, Q. J.; Huang, J. S.; Yang, X. Y. *Chem. Commun.* **2019**, *55*, 11551−11554.
(29) Zhang, Y.; Xu, G. Y.; Lian, G. L.; Luo, F.; Xie, Q. F.; Lin, Z. Y.; Chen, G. N. *Biosens. Bioelectron.* **2020**, *147*, 111789.
(30) Wen, Y. L.; Li, L. Y.; Li, J.; Lin, M. H.; Liu, G.; Liang, W.; Xu, L.; Li, Y.; Zuo, X. L.; Ren, S. Z.; Zhu, Y. *Anal. Chem.* **2020**, *92*, 4498−4503.
(31) Chang, Y.; Tang, X.; Huang, J.; Chai, Y.; Zhuo, Y.; Li, H.; Yuan, R. *Anal. Chem.* **2021**, *93*, 12075−12080.
(32) Yu, L. Y.; Zhu, L. P.; Yan, M. X.; Feng, S. N.; Huang, J. S.; Yang, X. R. *Anal. Chem.* **2021**, *93*, 11809−11815.